Transfer of orbital angular momentum to an optically trapped low-index particle

V. Garcés-Chávez,[1] K. Volke-Sepulveda,[1,2] S. Chávez-Cerda,[1,2] W. Sibbett,[1] and K. Dholakia[1,*]
[1]*School of Physics & Astronomy, University of St. Andrews, North Haugh, St. Andrews, Fife KY16 9SS, Scotland*
[2]*Grupo de Fotónica y Física Optica, INAOE, Apartado Postal 51/216, Puebla, Puebla 72000, Mexico*
(Received 20 August 2002; published 6 December 2002)

We demonstrate the transfer of orbital angular momentum from a light beam to a trapped low-index particle. The particle is trapped in a dark annular region of a high-order Bessel beam and rotates around the beam axis due to scattering from the helical wave fronts of the light beam. A general theoretical geometrical optics model is developed that, applied to our specific situation, corroborates tweezing and transfer of orbital angular momentum to the low-index particle. Good quantitative agreement between theory and experiment for particle rotation rates is observed.

DOI: 10.1103/PhysRevA.66.063402 PACS number(s): 32.80.Pj, 42.50.Vk, 42.60.Jf

I. INTRODUCTION

The linear momentum of light can be utilized to manipulate and trap microscopic objects. This is the result of the refraction and reflection of light at a dielectric interface which leads to changes in photon momentum and thus to a force being exerted on the trapped particle. In 1986 Ashkin and co-workers demonstrated that a single tightly focused optical beam could attract a high-index particle to the brightest part of the light beam due to the optical gradient force and trap the particle in three dimensions [1]. This powerful noninvasive technique is known as optical tweezers. Optical tweezers have found significant application in biology and chemistry. Several geometries using these optical forces have been proposed and implemented including optical levitation [2] and interferometric tweezers [3,4].

Low-index particles in optical tweezers have received relatively little attention. In contrast to high-index particles, they are repelled from light regions thus requiring more elaborate light beams for their confinement. Optical vortex beams such as Laguerre-Gaussian (LG) light beams have been used to trap low-index particles in three dimensions [5,6]. Simultaneous tweezing of low- and high-index particles in the axial direction has been demonstrated in such a system [7]. In recent work standard interferometric tweezers [4] were used to experimentally demonstrate tweezing of low-index particles obviating the need for optical vortex beams. In that work it was indicated that tweezing occurred when the particle diameter was larger than the fringe spacing of the interference pattern.

From a physical standpoint, optical tweezers have attracted significant interest from researchers studying the angular momentum of light. It is well known that light has spin angular momentum of magnitude $\hbar$ per photon due to its polarization state and orbital angular momentum of $l\hbar$ per photon due to an azimuthal phase term of the form $\exp(il\phi)$ in the mode description [8]. Here, l is the number of 2π cycles of optical phase upon going around the mode circumference. Orbital angular momentum (OAM) of light beams is a consequence of the azimuthal phase variation of certain light modes. Such modes have a term of the form $\exp(il\phi)$ and a concomitant orbital angular momentum in the direction of beam propagation [8]. These beams have a phase singularity along the beam axis and possess helical wave fronts. Indeed, we note that any light beam with helical wave fronts will have orbital angular momentum. The angular momentum of light can be calculated by $j=\epsilon_0[\mathbf{r}\times\langle\mathbf{E}\times\mathbf{B}\rangle]$, where j denotes the angular momentum density, $\mathbf{r}$ is a radius vector, and $\mathbf{E}$ and $\mathbf{B}$ are the electric and magnetic fields of the light field, respectively. This expression includes both contributions from the spin and orbital angular momentum of light.

Optical tweezers offer an excellent mechanism by which to study the angular momentum of light in detail and its manifestation in different experimental situations. Recent studies have included the transfer of spin and orbital angular momentum to trapped particles in optical tweezers [9,10]. In the case of orbital angular momentum this has been achieved due to both the scattering of light and absorption of the light [9,11–14]. All experiments to date studying angular momentum in optical tweezers have been for high-index particles attracted to regions of high light intensity or metallic particles. The motion of high-index particles in such experiments may be impeded by any azimuthal intensity variations in the light beams [12]. This is an obstacle, in the way of probing local variations in angular momentum density. Such density variations are predicted for more elaborate light fields [12,15] and can give deeper insight into both spin and orbital angular momentum.

In this paper, we demonstrate transfer of orbital angular momentum to a low-index particle. The low-index particle is trapped between adjacent bright rings of a high-order Bessel light beam [16] and has a larger diameter than the ring spacing of the Bessel beam. We observe azimuthal motion (rotation) of these particles around the Bessel beam propagation axis due to the orbital angular momentum of the light beam. The mechanism of transfer of OAM is scattering. In contrast to previous studies of transfer of orbital angular momentum, the trapped particle is localized primarily in the dark regions of the beam thus minimizing any heating or perturbative effects due to the light. Importantly, low-index particles could offer a mechanism for advanced studies of light beams possessing orbital angular momentum, notably local angular momentum variations in multiringed beams. Additionally, we

*Corresponding author. Email address: kd1@st-and.ac.uk

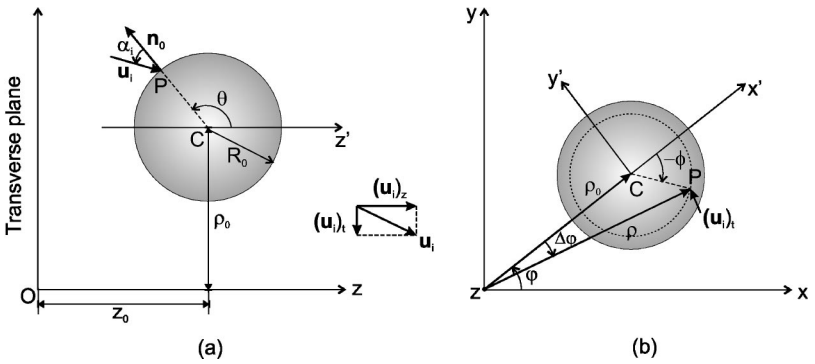

FIG. 1. Relevant geometrical parameters for our general ray tracing model for a spherical particle under the influence of a light beam propagating along the z direction.

observe rotation simultaneously of high- and low-index particles in our system.

Development and results of a numerical model are also presented. The model first verifies how tweezing can occur in a high-order Bessel beam and indeed confirms previous experimental studies of low-index particles in interferometric patterns [4]. Furthermore, the model allows us to calculate azimuthal forces on trapped spheres, and thus it shows how angular momentum can be transferred by scattering to the particle. In turn this permits quantitative comparisons between theory and experiment for rotation rates for microspheres set into motion by OAM.

II. THEORY

The forces exerted on a trapped particle can be modeled based on a geometrical optics approach, which has given very reliable results when compared with experiments (see, for example, [17–22]). Here, we use that approximation to analyze the angular momentum transfer by scattering from a high-order Bessel light beam to a trapped low-index particle that we will model with a hollow sphere. This is done by taking into consideration the azimuthal component of the linear momentum density of such a beam. We consider transparent media where absorption is neglected.

The ray-optics approach is valid if the particle diameter greatly exceeds the wavelength of light and the focal size of the beam. This is a reasonable assumption for our experimental parameters.

Within the geometrical optics approximation and following the same approach used by Gussgard and co-workers [19], the total force $\mathbf{F}$ acting on a transparent spherical particle due to an incident light beam can be expressed as

$$\mathbf{F}=\frac{n_m}{c}\int_{S_1} I(\mathbf{r})dA\cos\alpha_i\left\{\hat{\mathbf{u}}_i-R\hat{\mathbf{u}}_r-T^2\sum_{k=1}^{N}R^{k-1}\hat{\mathbf{u}}_{tk}\right\}, \tag{1}$$

where c/n_m is the light velocity in the medium surrounding the particle, S_1 is the part of the sphere's surface which is being illuminated by the incident field, $\hat{\mathbf{u}}_i$ and $\hat{\mathbf{u}}_r$ are unit vectors in the direction of the incident and reflected rays, respectively, $\hat{\mathbf{u}}_{tk}$ corresponds to the ray transmitted after the kth internal reflection, and $N\rightarrow\infty$ is the total number of internal reflections of the incident rays inside the sphere. R and T are the reflection and transmission coefficients derived from the Fresnel equations which, in accordance with Roosen [17], were taken as the averages over the two transverse directions of polarization relative to the plane of incidence for each illuminated element of the sphere. $I(\mathbf{r})$ is the intensity distribution of the incident field, in our case a high-order Bessel beam propagating along the z direction and $\mathbf{r}=(\rho,\varphi,z)$.

To evaluate expression (1) requires knowledge of the directions of all the reflected and transmitted rays, given the direction of the incident vector. We have developed a general ray tracing model, which allows us to perform this task by means of vectorial calculations for the case of a spherical particle [23].

A general outline of our model is described next. Consider a spherical particle of radius R_0 located at the point C of a coordinate system S referred to the light beam, whose origin corresponds to the center of symmetry of the transverse intensity distribution of the beam. A second reference frame S' is located at the center of the sphere, which is not fixed, but is moving along with the particle. Let ρ_0 be the distance between the z and z' axes, ρ the distance between the z axis and the incidence point P, and z_0 the distance between a reference plane $z=0$ and the center of the sphere. From Fig. 1 it can be seen that

$$\rho=[\rho_0^2+R_0^2\sin^2\theta+2\rho_0R_0\sin\theta\cos\phi]^{1/2}, \tag{2}$$

$$z=z_0+R_0\cos\theta, \tag{3}$$

where θ and ϕ are the polar and azimuthal angles in the S' coordinate system, respectively.

The unit outward normal to the sphere at the point P is given by

$$\hat{\mathbf{n}}_0=\hat{\mathbf{x}}'\cos\phi\sin\theta+\hat{\mathbf{y}}'\sin\phi\sin\theta+\hat{\mathbf{z}}'\cos\theta, \tag{4}$$

with $\hat{\mathbf{x}}'$, $\hat{\mathbf{y}}'$, and $\hat{\mathbf{z}}'$ being the unit vectors along the x', y', and z' directions in the S' frame.

Whether the unit vector in the direction of the incident ray at point P is denoted by $\hat{\mathbf{u}}_i$, the incidence angle can be calculated by means of

$$\cos\alpha_i=-(\hat{\mathbf{u}}_i\cdot\hat{\mathbf{n}}_0). \tag{5}$$

To calculate the reflected ray at the point of incidence $\hat{\mathbf{u}}_r$, we note that its component perpendicular to $\hat{\mathbf{n}}_0$ coincides

with the corresponding component of $\hat{\mathbf{u}}_i$, while its component along $\hat{\mathbf{n}}_0$ has the same magnitude but opposite sense to that of $\hat{\mathbf{u}}_i$. Hence by using Eq. (5), we have

$$\hat{\mathbf{u}}_r = \hat{\mathbf{u}}_i + 2\hat{\mathbf{n}}_0 \cos\alpha_i . \tag{6}$$

After some vectorial calculations and applying some geometrical considerations, we found for the transmitted ray into the sphere

$$\hat{\mathbf{u}}_t = \frac{n_m}{n_s}\left[\hat{\mathbf{u}}_i + \left(\cos\alpha_i - \frac{n_s}{n_m}\cos\alpha_t\right)\hat{\mathbf{n}}_0\right], \tag{7}$$

where α_t is the transmission angle and n_s and n_m are the refractive indices of the sphere and the medium, respectively, such that $n_s < n_m$.

On the other hand, for the rays transmitted out of the particle, we obtain, in general,

$$\begin{aligned}\hat{\mathbf{u}}_{t1} &= \frac{n_s}{n_m}\left[\hat{\mathbf{u}}_t - \left(\cos\alpha_t - \frac{n_m}{n_s}\cos\alpha_i\right)\hat{\mathbf{n}}_1\right],\\ \hat{\mathbf{u}}_{tk} &= \frac{n_s}{n_m}\left[\hat{\mathbf{u}}_{r\ k-1} - \left(\cos\alpha_t - \frac{n_m}{n_s}\cos\alpha_i\right)\hat{\mathbf{n}}_k\right],\end{aligned} \tag{8}$$

where the internally reflected rays are given by

$$\begin{aligned}\hat{\mathbf{u}}_{r\ 1} &= \hat{\mathbf{u}}_t - 2\hat{\mathbf{n}}_1\cos\alpha_t ,\\ \hat{\mathbf{u}}_{rk} &= \hat{\mathbf{u}}_{rk-1} - 2\hat{\mathbf{n}}_k\cos\alpha_t ,\end{aligned} \tag{9}$$

with k a positive integer such that $k>1$ and $\hat{\mathbf{n}}_k$ the unit normal to the sphere at the point where the kth reflection and refraction take place, given by

$$\begin{aligned}\hat{\mathbf{n}}_1 &= \frac{2n_m}{n_s}\cos\alpha_t\hat{\mathbf{u}}_i + \left(\frac{2n_m}{n_s}\cos\alpha_t\cos\alpha_i - \cos 2\alpha_t\right)\hat{\mathbf{n}}_0 ,\\ \hat{\mathbf{n}}_2 &= 2\cos\alpha_t\hat{\mathbf{u}}_t - (4\cos^2\alpha_t - 1)\hat{\mathbf{n}}_1 ,\\ \hat{\mathbf{n}}_k &= 2\cos\alpha_t\hat{\mathbf{u}}_{rk-2} - (4\cos^2\alpha_t - 1)\hat{\mathbf{n}}_{k-1} ,\end{aligned} \tag{10}$$

with $k>2$ for this last case.

By means of the recurrence relations (7)–(10), the direction of all the reflected and transmitted rays can be calculated in the last factor of Eq. (1). Please observe that we have imposed no condition over $\hat{\mathbf{u}}_i$.

We applied this model to each of the components of the vector that defines an incident ray for a high-order Bessel beam. In this instance the incident light vector may be obtained directly from the gradient of the phase of the beam

$$\frac{1}{k}\nabla\Psi(\rho,\varphi,z) = \frac{l}{k\rho}\hat{\varphi} + (\cos\gamma)\hat{\mathbf{z}}, \tag{11}$$

where $\Psi(\rho,\varphi,z) = l\varphi + (k\cos\gamma)z$ is the spatial phase of the beam, l its azimuthal order, k the wave number, γ the cone angle of the Bessel beam [24], and $\hat{\varphi}$, $\hat{\mathbf{z}}$, are the unit vectors in the azimuthal and axial directions, respectively. The propagation invariance of Bessel beams means, we have no radial component of the incident rays. As a consequence, Bessel beams only give two-dimensional traps and we thus concentrate only on transverse forces.

Inasmuch as the integration limits are different for the contributions to the optical force due to the azimuthal and the longitudinal components of the incident vector, it is necessary to treat them separately. Then, the total optical force can be written as the sum of both contributions, this is, $\mathbf{F}_t = \mathbf{F}^{(\varphi)} + \mathbf{F}^{(z)}$.

First, for the azimuthal incident rays, the unit vector can be expressed in the reference frame of the sphere as (see Fig. 1) $\hat{\varphi} = -\hat{\mathbf{x}}'\sin(\Delta\varphi) + \hat{\mathbf{y}}'\cos(\Delta\varphi)$, where $\Delta\varphi = \arccos[(\rho_0 + R_0\cos\phi\sin\theta)/\rho]$, so we can write

$$\hat{\varphi} = -\left[\frac{R_0\sin\phi\sin\theta}{\rho}\right]\hat{\mathbf{x}}' + \left[\frac{\rho_0 + R_0\cos\phi\sin\theta}{\rho}\right]\hat{\mathbf{y}}'. \tag{12}$$

Thus, by substituting Eqs. (12) and (4) in Eq. (5), we found for the incidence angle associated to an azimuthal incident ray

$$\cos\alpha_i = -(\hat{\boldsymbol{\varphi}}\cdot\hat{\mathbf{n}}_0) = -\frac{\rho_0\sin\phi\sin\theta}{\rho}. \tag{13}$$

The integration limits in Eq. (1) for this case are $\pi/2 \leqslant \theta \leqslant \pi$ and $\pi \leqslant \phi \leqslant 2\pi$, which corresponds to the illuminated area of the sphere by the azimuthal rays.

The explicit expression for the reflected rays $\hat{\mathbf{u}}_r$ is determined by substituting Eqs. (4), (12), and (13) in Eq. (6), while the transmitted vectors $\hat{\mathbf{u}}_{tk}$ are calculated numerically with the aid of the recurrence relations (7)–(10). Hence, the x' and y' components of the transverse optical force due to the contribution of the azimuthal incident rays $\mathbf{F}^{(\varphi)}$ are finally obtained

$$\begin{aligned}F_{x'}^{(\varphi)} = \frac{lR_0^2 n_m}{kc}\int_{\pi/2}^{\pi}\int_{\pi}^{2\pi}\frac{I_l(\mathbf{r})\rho_0\sin\phi\sin^2\theta}{\rho^2}\\ \times\left\{\sin\theta\left(T\frac{R_0}{\rho}\sin\phi - 2R\frac{\rho_0\sin\phi\sin\theta\cos\phi}{\rho}\right)\right.\\ \left. + T^2\sum_{k=1}^{N}R^{k-1}(\hat{\mathbf{u}}_{tk})_{x'}^{(\varphi)}\right\}d\phi d\theta,\end{aligned} \tag{14}$$

$$\begin{aligned}F_{y'}^{(\varphi)} = -\frac{lR_0^2 n_m}{kc}\int_{\pi/2}^{\pi}\int_{\pi}^{2\pi}\frac{I_l(\mathbf{r})\rho_0\sin\phi\sin^2\theta}{\rho^2}\\ \times\left\{T\left(\frac{\rho_0 + R_0\sin\theta\cos\phi}{\rho}\right) + 2R\frac{\rho_0\sin^2\theta\sin^2\phi}{\rho}\right.\\ \left. - T^2\sum_{k=1}^{N}R^{k-1}(\hat{\mathbf{u}}_{tk})_{y'}^{(\varphi)}\right\}d\phi d\theta,\end{aligned} \tag{15}$$

where $I_l(\mathbf{r})$ is the intensity distribution of an lth order Bessel light beam. In our experiment, we use an axicon generated

Bessel beam that has an intensity variation that can be approximated using the method of stationary phase applied to the Fresnel integral [25].

On the other hand, for the contribution of the axial rays to the transverse force $\mathbf{F}^{(z)}$, the incident vector should be taken as $\hat{\mathbf{u}}_i=\hat{\mathbf{z}}$, and the incidence angle reduces to $\pi-\theta$. The region of the particle that is illuminated by the axial rays is the lower hemisphere, hence, the integration limits are $\pi/2\leqslant\theta\leqslant\pi$ and $0\leqslant\phi\leqslant 2\pi$. And following a procedure completely analogous to the former case, we obtain for the x' component of the transverse optical force owing to the contribution of the axial incident rays

$$F_{x'}^{(z)}=\frac{R_0^2 n_m\cos\gamma}{2c}\int_{\pi/2}^{\pi}\int_0^{2\pi} I_l(\mathbf{r})\Bigg\{-2R\cos\theta\cos\phi + T^2\sum_{k=1}^{N} R^{k-1}(\hat{\mathbf{u}}_{tk})_{x'}^{(z)}\Bigg\}\sin 2\theta\, d\phi\, d\theta. \tag{16}$$

$\mathbf{F}^{(z)}$ have no component along y' because of the symmetry in the hemispheres defined by $0<\phi\leqslant\pi$ and $\pi<\phi\leqslant 2\pi$. Note that the Fresnel coefficients R and T, as well as the vectors $\hat{\mathbf{u}}_{tk}$, are not the same in Eq. (16), as in Eqs. (14) and (15), since they depend on the incidence angle [23].

Inasmuch as the total force acts on the center of mass of the sphere, we can summarize the above results by writing the net optical force in the transverse plane as $\mathbf{F}_t=F_\rho\hat{\rho}+F_\varphi\hat{\varphi}$, where $F_\rho\equiv F_{x'}^{(\varphi)}+F_{x'}^{(z)}$ and $F_\varphi\equiv F_{y'}^{(z)}$, since the x' and y' axes coincide with the radial and azimuthal directions of the S frame, respectively.

Finally, we want to stress that the model presented here is completely general and, provided an appropriate choice of the incidence vector and the initial intensity distribution, it can be simplified to more standard models in the literature [17,19], and to include others as particular cases [22]. In that sense, by establishing a comparison for previously studied situations, we found that by setting $N=20$, our results converge to those obtained with $N\to\infty$.

Figures 2 and 3 show, respectively, the radial and azimuthal components of the total force as a function of the distance from the center of the particle to the beam axis ρ_0, for a 5 μm diameter hollow sphere immerse in water ($n_w=1.333$, $n_s=1.0$). The beam parameters are $\lambda_0=1.064$ μm, $l=2$, and $\gamma=6°$ (which gives a peak radius for the inner bright ring of 3.5 μm, similar to our experimental values), a total power of $P=600$ mW and a maximum propagation distance of 1 mm. These plots were obtained for the z plane where the intensity has its maximum, at $z_{peak}=(\sqrt{2|l|+1}/2)z_{\max}$ [25], where $z_{\max}$ is the maximum propagating distance of a zeroth-order Bessel beam [24]. The intensity profile is also shown for comparison (gray curves).

According to the sign conventions we have adopted throughout this analysis, positive values of the radial quantities should be interpreted as being directed outwards from the center of the beam. Thus, for the radial component of the force, the stable equilibrium positions in Fig. 2 correspond to the points where $F_\rho(\rho_0)=0$ and the slope of the curve is negative, since for any displacement in a determined direction, there is a restoring force in the opposite direction that confines the particle in such points. As can be seen from Fig. 2 those equilibrium positions are located close to the dark zones of the beam, though the model predicts that they are slightly shifted outwards from the beam center.

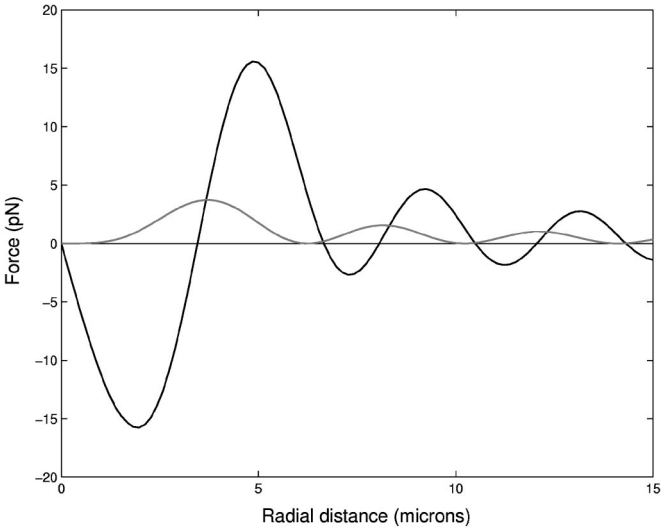

FIG. 2. The radial component of the total transverse force exerted by a Bessel light beam on a 5 μm diameter hollow sphere immersed in water, as a function of its distance from beam center (black curve) and beam intensity profile for comparison (gray curve).

This shifting of the equilibrium positions might be interpreted as a result of the imbalance between the intensity of consecutive bright rings, which pushes the hollow particle to the regions where the intensity is lower. In fact, we found that this behavior critically depends on the relative size of the particle with respect to the beam dimensions. The larger

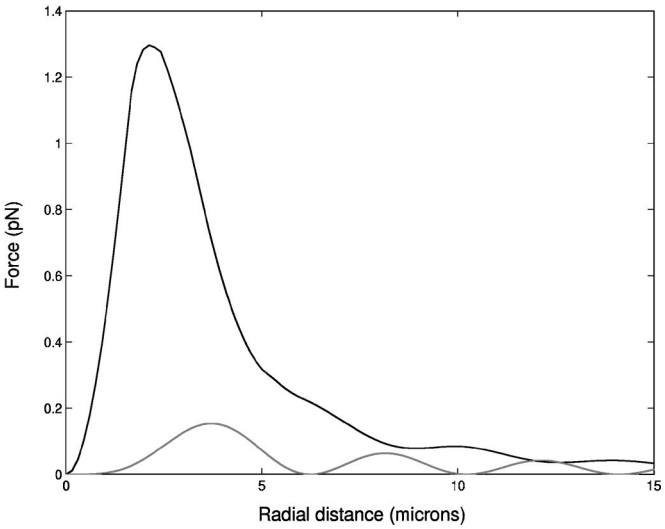

FIG. 3. The azimuthal component of the total transverse force exerted on a 5 μm diameter hollow sphere by a second-order Bessel beam (black curve) and beam intensity profile for comparison (gray curve).

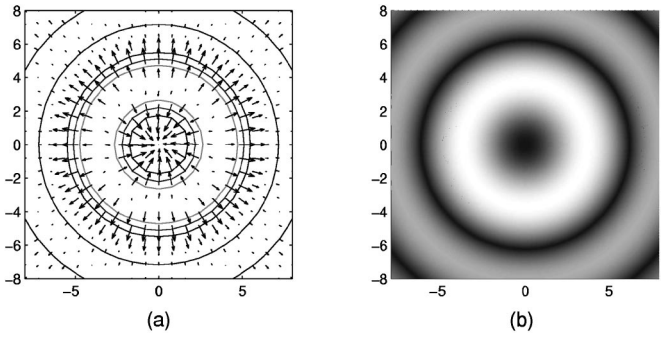

FIG. 4. In (a) we see a vector diagram showing the total transverse forces and contour curves. In (b) we see the corresponding Bessel beam profile.

the particle is, the more the equilibrium positions are shifted radially outwards, until a critical value for which the sphere can be trapped in the central minimum of the beam, but it cannot be stably trapped in any of the outer dark rings. This is in accordance with our experimental observations discussed later. For instance, with the same beam parameters we mentioned above, we found the critical value for the maximum diameter of the particle to be 6 μm, that is, a particle whose diameter is equal or larger than that value can only be held in the central minimum of the beam. In contrast, for a 5.75 μm diameter sphere, which can be trapped in any of the dark rings, we found that its equilibrium positions around the first and second dark rings are shifted about 16.6% and 7.2%, respectively, in relation with the corresponding minima of the intensity distribution. A 2 μm diameter sphere suffers a displacement of its equilibrium positions in the first and second dark rings of only 0.5% and 0.2%, respectively. The fact that the shifting in the equilibrium positions is lower for the second ring than for the first one can be understood by noting that the difference in intensity between consecutive rings decreases for regions further away from the beam center.

However, for smaller particles the geometrical optics approximation is no longer valid. Furthermore, it is important to mention that although in our experiments the hollow spheres have a finite shell width, we approximated this situation by considering the shell width negligible.

On the other hand, Fig. 3 shows that the azimuthal component of the force as a function of ρ_0, is always positive independent of the particle's radius, for hollow spheres. This result demonstrates that orbital angular momentum can indeed be transferred by scattering [12,14]. This fact is also valid for solid spheres trapped in the bright rings of the Bessel beam, as has been already demonstrated experimentally [12].

Combining the former results, the total transverse force is depicted in Fig. 4 for a 5 μm diameter hollow particle by means of a vector diagram and some contour curves of the beam profile. For comparison, the intensity of the corresponding beam is shown in Fig. 4(b). In the vector diagram, it can be appreciated that for the particle and beam parameters we have chosen, the equilibrium position close to the first dark ring is very weak in comparison with the central minimum of the beam, but again, this situation depends on the relative size between the particle and the transverse dimensions of the beam. The smaller the ratio between the particle's radius and the radius of the first bright ring of the beam, the more stable the equilibrium positions around the dark rings become. In addition, it can be seen in Figs. 2 and 3 that the magnitude of the azimuthal component of the force is several times smaller than that of the radial one, but this is enough to produce a vortex like distribution of the total force.

Finally, now we have determined the forces acting on the sphere due to the light beam, we can calculate the resulting torques along the propagating direction. The radial component of the net transverse force generates no torques on the particle with respect to the beam axis. Therefore, the sole torque on the particle is generated by the azimuthal component of the force, which is due to the orbital angular momentum of the beam. It can be expressed as $\tau_b = \rho_0 F_\varphi(\rho_0)$, when the particle is located at a distance ρ_0 from the beam axis.

However, the particle suffers also a drag torque due to its motion within the surrounding medium. Then, it reaches a constant angular velocity when both torques are balanced. The drag torque for a spherical particle can be estimated by means of the Stokes drag as $\tau_d = -6\pi\eta\rho_0^2 R_0 \omega_p$, with ω_p the angular velocity of the particle and η the viscosity of the surrounding medium, in this case $\eta = 1.0\times 10^{-3}$ N s m^{-2} for water at 20 °C. Hence, we can calculate the expected values for ω_p at the equilibrium positions, where the sphere orbits around the center of the beam with constant angular velocity, this is

$$\omega_p = \frac{F_\varphi(\rho_0)}{6\pi\eta\rho_0 R_0}. \tag{17}$$

Since $F_\varphi(\rho_0)$ is proportional to the incident power of the beam via the $I(\mathbf{r})dA$ factor in Eq. (1), Eq. (17) implies a linear behavior of the angular velocity as a function of the incident power. Such behavior has been seen in recent work where a linear relationship between rotation rate and incident power was observed experimentally for rotation of 3 μm solid spheres [12]. We show in Fig. 5 the results of our model compared with the experimental data for solid spheres and find very good agreement. To the best of our knowledge, this constitutes the first quantitative measurements between theory and experiment for orbital angular momentum transfer to trapped particles. In the following section, we demonstrate the rotation of hollow spheres due to OAM and compare the results with our model.

III. EXPERIMENT

We used an optical tweezers system similar to the one described previously [12,26]. We expand a linearly polarized Gaussian output beam of a cw Nd:YVO_4 laser (1.5W at 1.064 μm) to illuminate a computer-generated hologram. This blazed phase hologram diffracted about 80% of the incident light into a first-order beam with helical wave fronts, giving a close approximation to a Laguerre-Gaussian beam with azimuthal mode index $l=2$ in the far field. This beam illuminated an axicon having an opening angle of one de-

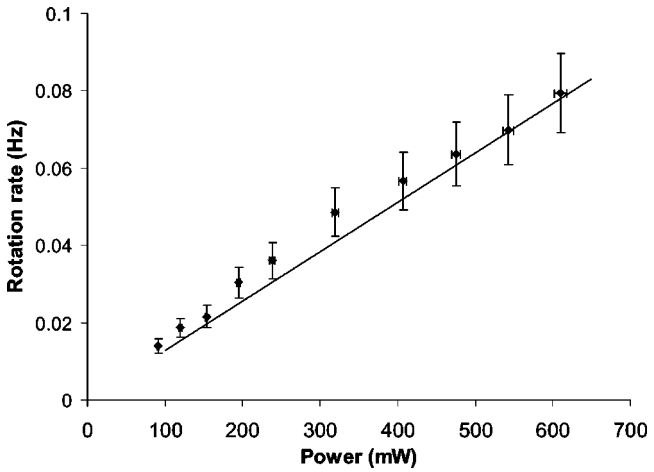

FIG. 5. Rotation rates for 3 μm high-index silica sphere in a Bessel beam (from Ref. [12]). The fit to the data (solid line) is from our model and shows good agreement. We stress that this fit is with no free parameters.

gree, thus generating an approximation to a higher-order Bessel beam [16]. A telescope ($\times 1/20$) was used to reduce the radius of the first (inner) ring of the Bessel beam. This also resulted in a reduced propagation distance of the Bessel beam and increased its intensity. For a beam of azimuthal mode index $l=2$ the inner ring of the imaged Bessel beam had a peak radius of about 2.9 μm and propagated for ≈ 1 mm. This beam was directed downwards onto the sample mounted on an translation stage. A microscope objective ($\times 60$) and charge-coupled device camera were placed below the sample for observation of the particles.

The propagation distance of our higher-order Bessel beam is fairly short and the peak intensity of the beam varies along this propagation distance. Therefore, the vertical positioning of the sample cell along the propagation direction is important. The sample is positioned in the plane with the highest peak intensity in the inner ring. Experimentally, this was achieved by placing the sample stage in the z position where the transverse trapping of the hollow spheres was strongest. The maximum laser power in the sample plane was about 600 mW. As all the rings of a Bessel beam contain a similar amount of its total power this corresponds to ≈ 15 mW in each of the 40 rings of our experimental Bessel beam.

The alignment of the whole optical system was critical, as even slight astigmatism can lead to a loss of the symmetrical beam profile and a breakup of the central vortex of the beam. The quality of the Bessel beam is very important because any intensity variation around the central ring hinders the continuous rotation of trapped particles [12]. Low-index (hollow) microspheres (Duke Scientific USA) with diameters from 2 μm to 20 μm were dispersed in water with a minute amount of detergent added to aid mobility. The hollow spheres had a shell thickness of $\approx 5\%$ to 10% of their total diameter.

IV. RESULTS

The downwards direction of the beam directed the hollow spheres by scattering to the bottom of the sample slide. As

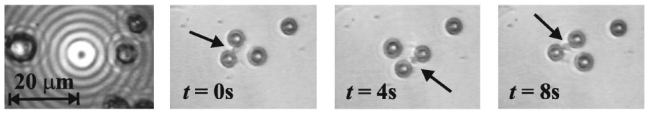

FIG. 6. Tweezing and rotation of three low-index spheres in a high-order Bessel beam.

expected, we were readily able to tweeze the hollow spheres in the central minimum of the Bessel light beam. Furthermore, we were able to tweeze hollow spheres in regions away from the center of the beam. Specifically, we trapped the spheres in two dimensions in the dark regions between adjacent rings of the Bessel light beam (Fig. 6) as predicted by our model, thus creating two dimensional circularly symmetric arrays of hollow spheres. This behavior is consistent with earlier observations of tweezing hollow spheres in the dark regions of an interferometric pattern between two Gaussian light beams [4]. The equilibrium positions were noted for spheres to be radially displaced in accordance with our model though direct comparison was difficult due to the accuracy of our measurements and the finite shell width of the spheres. In addition, we have observed the simultaneous transfer of orbital angular momentum to both high- and low-index particles. In Fig. 7, we can see a single high-index particle trapped in the bright inner ring rotating due to scattering and simultaneously, we can see a low-index particle trapped and rotating between the bright rings. The first frame shows the Bessel beam and where the hollow and solid sphere are trapped. Hollow spheres that were tweezed between the first and second bright ring of the Bessel light beam were observed consistently to rotate around the beam propagation axis (Figs. 6 and 7). The direction of rotation was consistent with the measured helicity of the Bessel beam. The sense of rotation of the particles was reversed when the helicity of the Bessel beam was reversed using a Dove prism. The rotation of the particles is due to the helical phase fronts of the high-order Bessel beam and shows transfer of orbital angular momentum to low-index particles. The behavior is also in accordance with the notion of the hollow sphere interacting with the extrinsic orbital angular momentum of the beam [14]. We also found that the uniformity of the Bessel beam was not as critical as when dealing with high-index particles [12]. High-index particles are attracted

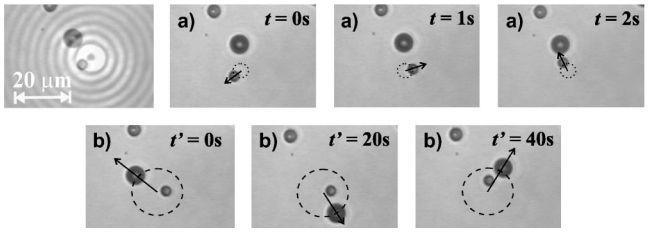

FIG. 7. Tweezing and rotation around the beam axis of both a high- and low-index particle simultaneously in a high-order Bessel light beam. The figure in the top left shows the Bessel beam and the large hollow sphere and solid (high index) particle. The top row [frames (a)] show rotation of the solid sphere (about 2.5 μm diameter) and the bottom row [frames (b)] rotation of a hollow sphere. The time scales for rotation of each particle are indicated.

to the regions of high light intensity and their rotation is significantly influenced by azimuthal intensity variations. Such hot spots of intensity can impede the azimuthal motion of the particle causing it to be locally tweezed at some point on the beam circumference. For low-index particles however the case is different as they are localized to the dark regions between the rings of the Bessel beam. Intensity variations in this instance can cause a small radial motion that accompanies the azimuthal rotation of the particles. In all instances, however, we found that beam imperfections (azimuthal intensity variations up to 20%) did not impede the rotation of low-index particles. This is in contrast to high-index particles. We measured the particle rotation rate as a function of power and found a linear response (Fig. 8). In this instance, we used a telescope ($1/16\times$) to obtain a beam where the peak radius of the inner ring was 3.5 μm. The radius of the first dark ring was ≈ 6 μm. The graph represents data for several sizes of sphere from 5–6 μm in diameter. A range was taken to include any errors due to finite shell width. The fit shows good agreement between experiment and theory. This confirms the linear relationship between the power and the rotation rates implied in Eq. (17).

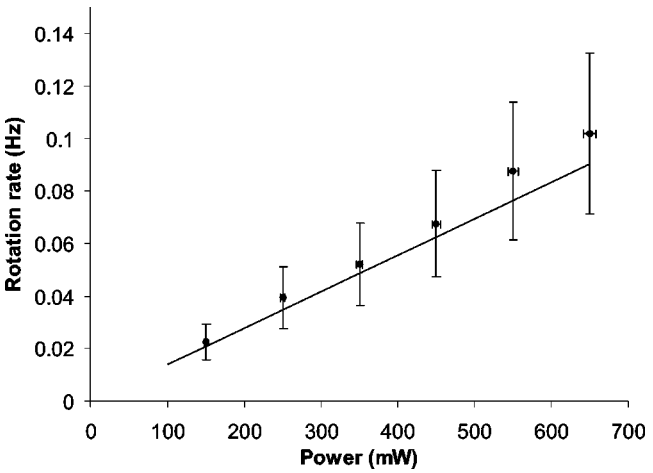

FIG. 8. Rotation rates as a function of the total incident power. The radius of the first bright ring was about 3.5 μm and the radius of the first dark ring was about 6 microns, respectively, for these data. The linear graph shows that the angular momentum of each photon must be proportional to $l\hbar$. The data are fitted to our model (taking the ideal hollow sphere size as 5.5 μm) with no free parameters. The good agreement shows the validity of our model as does Fig. 5.

V. CONCLUSIONS

We have demonstrated the transfer of orbital angular momentum to a low-index particle trapped in optical tweezers. The particle is constrained to the dark regions between adjacent bright rings of a high-order Bessel beam. Additionally we have observed both high- and low-index particles rotating due to OAM in our system. Particle rotation rates are consistent with a computer model developed based on the scattering as the dominant mechanism for transfer of OAM. Although our model was only applied to the case of high-order Bessel beams, it is more general and can be applied to any kind of beam. Our quantitative comparison between theory and experiment shows very good agreement for rotation rates. Low-index spheres may offer an exciting avenue for a detailed study of local angular momentum variations in multiringed light beams such as high radial index LG beams and Bessel beams. These particles respond to the orbital angular momentum of the light but are relatively insensitive to azimuthal variations in intensity.

ACKNOWLEDGMENTS

We would like to thank the Leverhulme Trust, the U.K. Engineering and Physical Sciences Research Council and CONACYT, Mexico for their support of our work and D. McGloin for critical reading of the manuscript.

[1] A. Ashkin, J. Dziedzic, J. Bjorkholm, and S. Chu, Opt. Lett. **11**, 288 (1986).
[2] A. Ashkin and J.M. Dziedzic, Appl. Phys. Lett. **28**, 333 (1976).
[3] A.E. Chiou, W. Wang, G.J. Sonek, J. Hong, and M.W. Berns, Opt. Commun. **133**, 7 (1996).
[4] M.P. MacDonald, L. Paterson, W. Sibbett, K. Dholakia, and P.E. Bryant, Opt. Lett. **26**, 863 (2001).
[5] K.T. Gahagan and G.A. Swartzlander, Jr., Opt. Lett. **21**, 827 (1996).
[6] K.T. Gahagan and G.A. Swartzlander, Jr., J. Opt. Soc. Am. B **15**, 524 (1998).
[7] K.T. Gahagan and G.A. Swartzlander, Jr., J. Opt. Soc. Am. B **16**, 533 (1999).
[8] L. Allen, M.W. Beijesbergen, R.J.C. Spreeuw, and J.P. Woerdman, Phys. Rev. A **45(11)**, 8185 (1992).
[9] H. He, M.E.J. Friese, N.R. Heckenberg, and H. Rubinsztein-Dunlop, Phys. Rev. Lett. **75(5)**, 826 (1995).
[10] M.E.J. Friese, T.A. Niemenen, N.R. Heckenberg, and H. Rubinsztein-Dunlop, Nature (London) **394**, 348 (1998).
[11] N.B. Simpson, K. Dholakia, L. Allen, and M. Padgett, Opt. Lett. **22**, 52 (1997).
[12] K. Volke-Sepulveda, V. Garcés-Chávez, S. Chávez-Cerda, J. Arlt and K. Dholakia, J. Opt. B: Quantum Semiclassical Opt. **4**, S82 (2002).
[13] A.T. O'Neil and M.J. Padgett, Opt. Commun. **184**, 139 (2000).
[14] A.T. O'Neil, I. McVicar, L. Allen, and M.J. Padgett, Phys. Rev. Lett. **88**, 053601 (2001).
[15] L. Allen and M.J. Padgett, Opt. Commun. **184**, 67 (2000).
[16] J. Arlt and K. Dholakia, Opt. Commun. **177**, 297 (2000).
[17] G. Roosen and C. Imbert, Phys. Lett. **59A**, 6 (1976).
[18] G. Roosen, Opt. Commun. **21**, 189 (1977).
[19] R. Gussgard, T. Lindmo, and I. Brevik, J. Opt. Soc. Am. B **9**, 1922 (1992).
[20] A. Ashkin, Biophys. J. **61**, 569 (1992).
[21] Shojiro Nemoto and Hiroyoshi Togo, Appl. Opt. **37**, 6386 (1998).

[22] R.C. Gauthier and S. Wallace, J. Opt. Soc. Am. B **12**, 1680 (1995).
[23] K. Volke-Sepulveda, V. Garcés-Chávez, K. Dholakia, S. Chávez-Cerda (unpublished).
[24] J. Durnin, J.J. Miceli, and J.H. Eberly, Phys. Rev. Lett. **58**, 1499 (1987).
[25] J. Arlt, K. Dholakia, J. Soneson, and E.M. Wright, Phys. Rev. A **63**, 063602 (2001).
[26] J. Arlt, V. Garcés-Chávez, W. Sibbett, and K. Dholakia, Opt. Commun. **197**, 239 (2001).